Neutron scattering from equilibrium-swollen networks

S.K. Sukumaran[1,a], G. Beaucage[1,b], J.E. Mark[2], and B. Viers[2]

[1] Department of Materials Science and Engineering, University of Cincinnati, Cincinnati, OH 45221-0012, USA
[2] Department of Chemistry, University of Cincinnati, Cincinnati, OH 45221-0172, USA

Abstract. Small-angle neutron scattering measurements were performed on end-linked poly (dimethyl-siloxane) (PDMS) networks swollen to equilibrium with d-benzene. Comparison was made with equivalent concentration PDMS solutions. Equilibrium-swollen networks consistently displayed a linear scattering regime at low q followed by a good-solvent–like scaling regime at high q in agreement with the predictions of the Gel Tensile Blob (GTB) model. Data are fit using the unified function modified for the GTB model (3-parameter fit). Equilibrium-swollen networks display a base structural size, the gel tensile-blob size, ξ, that was found to be independent of the molecular weight between crosslinks for the series of molecular weights studied, consistent with the predictions of the model. The length of the extended tensile structure, L, can be larger than the length of the fully extended network strand. The predicted scaling relationship for L, $L \sim Q^{1/2}N_{\mathrm{avg}}$, where $N_{\mathrm{avg}} = \left(1/fN_{\mathrm{c}}^2 + 1/4N_{\mathrm{e}}^2\right)^{-1/2}$, Q is the equilibrium swelling ratio, N_{c} is the molecular weight between crosslinks, N_{e} is the entanglement molecular weight and f is the crosslink functionality is in agreement with experimental results for the networks studied.

PACS. 61.41.+e Polymers, elastomers, and plastics – 82.70.Gg Gels and sols – 61.12.Ex Neutron scattering techniques (including small-angle scattering)

1 Introduction

The physics of polymer gels far above the gelation threshold has long been an active field of study [1–3]. The classical theories for the equilibrium swelling of a network in a good solvent, the Flory-Rehner theory [1] and the de Gennes c* theorem [2], predict that the structural properties of the gel are solely determined by the average size of the polymer chain between crosslinks (the mesh size). According to these theories, scattering from a polymer gel arises solely due to thermal fluctuations of the polymer concentration and the scattered intensity at low q from the swollen gels should not be very different from that of a semi-dilute solution at the same concentration [4,5]. Also, the scattered intensity should saturate above the mesh size, similar to the screening effect in semi-dilute solutions [3,4]. It became evident, mainly from scattering experiments that the internal structure of gels is more complicated than that suggested by the classical theories.

Evidence for disagreements between the gel structure revealed by scattering data and the predictions of the classical theories has accumulated since the 1970s. Early light scattering experiments by Bueche [6], Pines and Prins [7],

Wun and Prins [8] and Stein *et al.* [9] revealed that, in several cases, the absolute scattered intensity from the gel was significantly higher than the thermodynamic predictions based on the Flory-Rehner theory. The increase in the intensity was attributed to quenched heterogeneities in the structure of the gel although the authors disagreed over the origin of these heterogeneities. Joosten, McCarthy and Pusey [10], by scanning a gel sample with a laser beam, were able to separate the contributions to the total intensity into ensemble-averaged (solid-like) and fluctuating (liquid-like) components. The results of the experiment strongly suggest, at least for the system studied (poly (acrylamide) gels), that the enhancement of intensity is mainly due to quasi-static fluctuations in polymer concentration, which in turn, were attributed to the frozen heterogeneities in the system.

Several research groups have used small-angle neutron scattering experiments to investigate the internal structure of polymer gels [11–18]. Earlier experiments [11–13] cast serious doubts on some of the assumptions involved in the Flory-Rehner theory (for a discussion see the introduction to our earlier paper [19]). It should be noted that neutron scattering measurements based on tagged chains between crosslinks and tagged crosslink sites [11–13] fail to display large-scale structural features. The excess scattering has been observed in gels made from several polymeric

---

[a] *Present address*: Max-Planck-Institute for Polymer Research, PO Box 3148, Mainz, Germany.
[b] e-mail: `beaucag@uc.edu`

species and thus appears to be species independent [14–18]. Several analytical functions have been proposed to analyze scattering data from polymer gels [16,17,20–22]. Falcao *et al.*, consider the gel as a fractal aggregate of particles [16]. The particles were identified with concentration blobs in a semi-dilute solution and an empirical form factor was proposed. Geissler *et al.* [17] used the sum of a stretched exponential and a Lorentzian to fit the scattering curve from a swollen network. Both the approach of Geissler *et al.* and that of Falcao *et al.*, although largely empirical, yield reasonable fits to the scattering data. Bastide and Leibler [20], using an analogy with percolation clusters, derived an expression for the scattering intensity that was essentially a Lorentzian modified by a crossover function. Onuki [21], by considering quenched heterogeneities as small perturbations in a linear elasticity theory of the gel, obtained independent functions to describe both the contribution due to the quenched fluctuations (which includes a parameter that describes the heterogeneities) and the thermal fluctuations. Using this scattering function to analyze the data leads to quantitative inconsistencies between various predictions of the theory. Also, as already pointed out by the author himself [21], there is no reason to expect the heterogeneities to act as a small perturbation and indeed estimates of the heterogeneity parameter obtained by using Onuki's scattering function lead to large values. Panyukov and Rabin have proposed a theory for polymer gels [22] and the predicted scattering functions were used to analyze data from poly(N-isopropylacrylamide) gels in [23]. It was found [23] that the predicted scattering functions reproduced the experimental curves satisfactorily. However, it should be borne in mind that the Panyukov-Rabin theory treats the polymer strands as phantom chains and hence physical interactions between chains like trapped entanglements are not considered.

In a previous paper by two of the authors [19], a structural model to describe the scattering data obtained from equilibrium-swollen polymer networks was introduced. This was accomplished by a generalization of the tensile-blob construction for a linear polymer, introduced by Pincus [24], to structural elements of arbitrary connectivity. Two characteristic size scales for the structure of a polymer gel, the gel tensile-blob size, ξ, and a large scale length, L, were predicted. The large-scale structure, L, resulted from a force balance between the network elasticity and enthalpic swelling, mitigated by random topological clusters in the network. The effect of trapped entanglements on the swelling behavior was included in the model and yielded scaling predictions for both ξ and L. It was proposed that

$$\xi \sim \frac{l}{(1-2\chi)^P}, \text{ where } P = \frac{2-(D+\alpha)}{((D+\alpha)(4+d)-2d)} \quad (1)$$

and l is the persistence length, χ is the Flory-Huggins interaction parameter, D is an internal dimension of the network, α characterizes the degree of interpenetration in the network and d is the spatial dimension. L was pre-
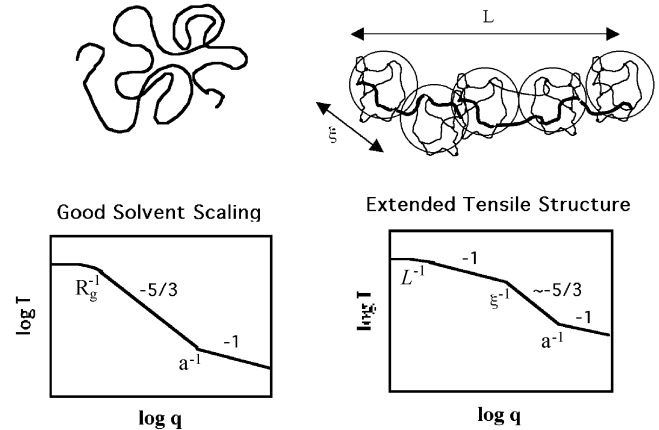
Fig. 1. Top, cartoon of a single chain in dilute solution (left) and the schematic of the extended tensile structure following the GTB model (right) [19]. ξ is the tensile-blob size and L is the extended length. Bottom, schematic of scattering patterns resulting from the structures shown at top. "a" is the persistence length, R_g is the overall radius of gyration of the single chain, ξ is the gel tensile-blob size and L is the length of the extended tensile structure.

dicted to follow,

$$L \sim Q^{1/2} N_{avg}, \text{ where } N_{avg} = \left(\frac{1}{fN_c^2} + \frac{1}{4N_e^2}\right)^{-1/2} \quad (2)$$

and Q is the equilibrium swelling ratio ($Q = 1/\phi$, ϕ being the polymer concentration), N_c is the molecular weight between crosslinks, N_e is the entanglement molecular weight and f is the crosslink functionality. A schematic of the large-scale structure in the gel and the expected scattering curve for the structure is shown in Figure 1. The corresponding figures for a polymer chain in solution are also shown for comparison.

In this article the structural validity of the GTB model, as presented above, is explored using neutron scattering measurements from equilibrium-swollen networks. The GTB model is used to define a 3-parameter fitting function based on the unified equation [25–27] that yields the extended length, L, diameter, ξ, and contrast from the scattering pattern. The proposed function is used to analyze the neutron scattering data from equilibrium-swollen poly (dimethylsiloxane) networks. The predictions of the GTB model are then compared with experimental data.

2 Experimental

A series of model end-linked poly (dimethylsiloxane) (PDMS) networks of variable N_c were prepared by two crosslinking techniques, hydrosilation crosslinking using a platinum catalyst and vinyl-terminated PDMS, and condensation reactions using tetraethylorthosilicate (TEOS), hydroxyl-terminated PDMS and dibutyl tin dilaurate catalyst. The vinyl crosslinking results in ideally small crosslink sites and no byproduct. The condensation reaction leads to bulkier crosslink sites and ethanol as a

byproduct. Both of these crosslinking reactions are described in detail in the PhD dissertation of B. Viers [28]. Table 1, below, lists the various molecular weights between crosslinks that were used. These values were determined using gel permeation chromatography [28]. Both reactions are expected to yield tetrafunctional crosslink sites.

Equilibrium swelling of the samples was performed on monolithic pieces of the networks formed from either the hydrosilation or condensation reactions. The samples were swollen in benzene and allowed to equilibrate. The benzene solvent was changed daily and the weight was measured until there was no change in the weight for a few days. The samples were then deswollen in successive benzene/methanol solutions of increasing methanol content until the sample was completely deswollen in methanol. The samples were then dried in a vacuum oven and weighed [28]. The equilibrium volume fraction of rubber in the benzene-swollen sample was calculated assuming additivity of volumes from the equilibrium-swollen weight and the dried weight using a density for PDMS of 0.98 g/cm^3 and 0.878 g/cm^3 for benzene at room temperature. In general the soluble fraction was 10% or less during the rinsing stages.

Neutron scattering experiments were performed on equilibrium-swollen PDMS networks and equivalent linear chains at the same polymer concentration, in perdeuterated benzene (d-benzene) at 25 °C using the Small-Angle Neutron Diffractometer (SAND) at the Intense Pulsed Neutron Source (IPNS), Argonne National Laboratory, or the 8-meter SANS instrument at the National Institute of Standards and Technology. The angular range of the SAND instrument is recognizably broader than the 8-meter instrument at NIST (Fig. 4 below). The scattering data were corrected for empty cell and solvent scattering, detector sensitivity, and sample transmission using routine correction procedures available at both facilities. The differential scattering cross-section $I(q)$ was placed on an absolute scale in the units of cm^{-1} by using secondary standards whose absolute scattering cross-sections are known. Finally, incoherent scattering was measured and subtracted.

3 GTB Model and the unified function

The schematic of the scattering pattern from the extended tensile structure, Figure 1, exhibits several power law scattering regimes. In a scattering plot, a change in the power law exponent —visually, a change in the slope in a log-log plot— will be referred to as a "scaling transition" in this work. For scattering patterns exhibiting scaling transitions, it is convenient to view the scattering pattern or, equivalently, the structure of the system itself, as composed of "structural levels". This viewpoint is implicit in using the unified function [25–27], which describes small-angle scattering from systems exhibiting scaling transitions in terms of structural levels. A structural level consists of a Guinier regime, corresponding to the average size of the structure and the associated power law regime

that continues from the Guinier regime in q-space. Limits to the power law regime at low q are based on generic power law functions, but with a cut off at large sizes incorporated in them. The adoption of such a limit at the large size directly leads to the use of the radius of gyration to limit the power law function in a general way, *i.e.* the functional form of this limit does not depend on the exponent of the power law decay (for an elaboration of this point see ref. [27]). On the other hand, the high-q limit to the power law at a scaling transition is essentially adopted form previous work (of Guinier, for example). For scaling transitions (such as at the tensile-blob size, ξ), the high-q limit to power laws can also be calculated in a generic fashion [26]. The unified function is then composed of a series of discrete scaling regimes, each of which has an associated radius of gyration, R_{gi}, contrast factor, G_i, power law slope, P_i, and power law prefactor, B_i, where the index, i, is used to label the structural levels, starting with 1 for the structural level at the highest q. These 4 parameters can be directly limited by models assumed for the structure. A rod of sufficient aspect ratio ($L/R > 3.3$, where L is the length and R the radius of the rod) displays two structural levels associated with the radius and the length [29]. The larger radius of gyration, R_{g2}, seen at low q, is given in terms of L and R, as

$$R_{g2}^2 = \frac{L^2}{12} + \frac{R^2}{2}. \tag{3}$$

For the tensile structure, $2R \approx \xi$.

There are two ways of relating the diameter of the extended tensile structure, ξ, to its radius of gyration at small size scales. If we consider the tensile structure strictly as a rod, then the smaller R_g, R_{g1}, is the radius of gyration for a rod of radius, R, and is given by $R_{g1}^2 = 3R^2/4$ [29]. This leads to $\xi \approx 2R = 2.31\, R_{g1}$. If instead we consider the tensile blob as a mass fractal object, its radius of gyration, R_{g1}, is related to its end-to-end distance, ξ, by [26]

$$\xi^2 = R_{g1}^2 \left(1 + \frac{2}{d_f}\right)\left(2 + \frac{2}{d_f}\right) \tag{4}$$

Assuming good-solvent scaling for the chains in the blob, *i.e.* $d_f \approx 5/3$, results in $\xi = 2.65 R_{g1}$. In this paper we have used equation (4) for calculating ξ from R_{g1}.

As the persistence length [26] is not observed in the scattering data from the gels studied in this work (see Figs. 2 and 3), the unified function for the GTB model consists of two structural levels and is written as

$$I(q) = \left\{ G_2 \exp\left(-\frac{q^2 R_{g2}^2}{3}\right) + B_2 \exp\left(-\frac{q^2 R_{g1}^2}{3}\right)(q_2^*)^{-1} \right\}$$
$$+ \left\{ G_1 \exp\left(-\frac{q^2 R_{g1}^2}{3}\right) + B_1 (q_1^*)^{-d_f} \right\}, \tag{5}$$

where

$$q_i^* = \frac{q}{\left\{ \mathrm{erf}\left(\frac{q R_{gi}}{\sqrt{6}}\right) \right\}^3}. \tag{6}$$

The function in (5) for the GTB model uses 8 generic parameters (4 for each of 2 structural levels), which can be further limited to only 3 parameters by constraints inherent to the GTB model, as described below.

3.1 Level 1, gel tensile blob (subscript 1 in (5))

This structural level pertains to the gel tensile blob. For this level, B_1 is given by [26]

$$B_1 = \left(\frac{G_1 d_{\mathrm{f}}}{R_{\mathrm{g1}}^{d_{\mathrm{f}}}} \right) \Gamma \left(\frac{d_{\mathrm{f}}}{2} \right) , \qquad (7)$$

where, $\Gamma()$ is the gamma-function and

$$G_1 = c N_{\mathrm{blob}} \left(g_{\mathrm{p}} \Delta \rho \right)^2 , \qquad (8)$$

where g_{p} is the number of persistence units in a tensile blob, $\Delta \rho$ is the contrast per persistence unit, N_{blob} is the number of tensile blobs in one extended tensile structure, and c is the number of extended tensile structures per unit scattering volume.

3.2 Level 2, extended tensile structure

This structural level pertains to the extended tensile structure composed of the tensile blobs. For the 1d extended structure of the GTB model, B_2 can be obtained from [26]

$$B_2 = \left(\frac{G_2}{R_{\mathrm{g2}}} \right) \Gamma \left(\frac{1}{2} \right) , \qquad (9)$$

or from scattering function for a long rod as $B_2 = \pi G_2 / L$. G_2 is defined as

$$G_2 = c \left(N_{\mathrm{blob}} g_{\mathrm{p}} \Delta \rho \right)^2 = N_{\mathrm{blob}} G_1 , \qquad (10)$$

and R_{g2} is defined above (Eq. (3)) in terms of L and ξ. B_2 calculated using mass fractal laws [26] is $1.77\, G_2 / R_{\mathrm{g2}}$, and from the rod function [28] it is $0.91 G_2 / R_{\mathrm{g2}}$ if $L \gg \xi$. The function given in equation (9) was used to calculate B_2 in the fits presented here. N_{blob} is defined here as $N_{\mathrm{blob}} = L/\xi$, so that only one of G_1 or G_2 needs to be a free parameter.

Using the GTB model to limit the unified function yields a function with only *3 free parameters*, G_2, R_{g2} and R_{g1}. Using the above relationships, these three parameters yield L, ξ, $(c^{1/2} g_{\mathrm{p}} \Delta \rho)$ and N_{blob}.

4 Results/Discussion

Figure 2 shows small-angle neutron scattering patterns obtained at the Argonne National Laboratory from two equivalent samples. The top curve (hollow triangles) is the scattering from a network of 22000 g/mole PDMS, end-linked by reaction of vinyl terminal groups as described above [25]. The network was swollen to equilibrium in
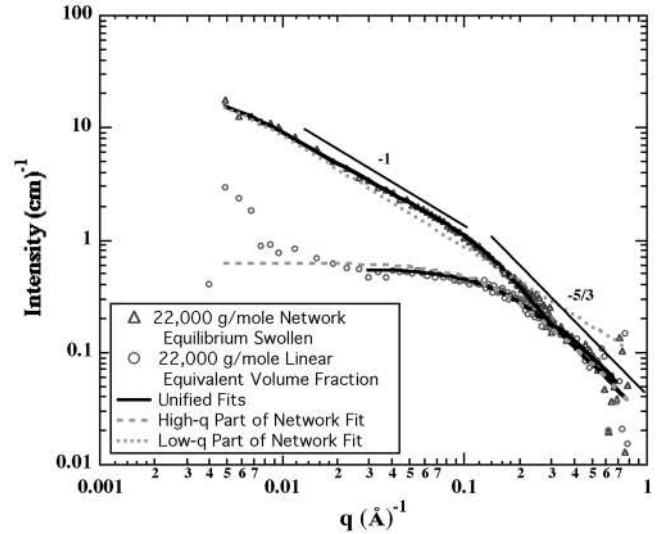
Fig. 2. 22000 g/mole PDMS equilibrium-swollen network *versus* equivalent solution. The concentration blob occurs at $R_{\mathrm{g}} = 8.88 \pm 0.04$ Å; and the tensile blob at $R_{\mathrm{g}} = 7.8 \pm 0.2$ Å. The data is from Argonne National Laboratories SAND instrument. The fit is to the unified equation [25–27] using the GTB model as described in the text and appendix.

d-benzene. The bottom curve (open circles) is the scattering from an equivalent solution, same volume fraction, of uncrosslinked polymer. The equivalent solution sample can be visualized as close-packed concentration blobs and hence is uniform at size scales larger than the concentration blob size [2]. Therefore, for q values corresponding to length scales larger than the concentration blob size, the system displays flat scattering. On the other hand, in the network sample, at large scales of observation, this homogeneity is not seen since the chains in the equilibrium-swollen network are presumably stretched into the extended tensile structures, as was argued in a previous paper [19]. Scaling above the gel tensile-blob size, ξ, *i.e.* at lower q, is linear consistent with the GTB model. At high q, a scaling regime, with a scaling exponent roughly equal to 5/3 is observed, similar to a polymer in dilute solution. The transition between these two scaling regimes is related to the tensile-blob size, ξ. This size is obtained from a radius of gyration in the unified fit [25–27] as explained in the previous section. In cases where the extended tensile structure, L, becomes comparable in size to the tensile blob, ξ, a clear linear decay at low q may become obscured, as in the lower four curves in Figure 3, and Figure 4. The 3-parameter unified fit can still be used to obtain L and ξ using the GTB model even in such cases as illustrated in Figure 4.

In Figure 2, top curve, the unified fit is composed of two structural levels, one pertaining to the gel tensile blob at high q and one pertaining to the linear string of tensile blobs at low q. The contribution to the scattered intensity from these two levels of structure can be plotted independently in the unified approach by considering two single-level unified scattering functions, the light dashed
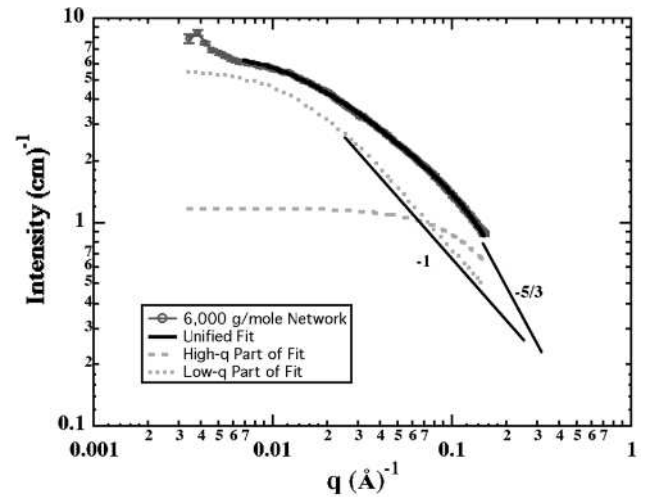
Table 1. Fit parameters for the GTB. Falcao parameters are obtained from fits to the data of reference [16]. (Falcao *et al.* used p-xylene rather than benzene.)

Molecular weight, g/mole (N)	Crosslink agent	R_g extended Å	R_g tensile blob Å	Extended length L, Å	Tensile blob size ξ, Å	G_2, cm^{-1}	Q_{eq}
300 (4)	TEOS	41.1	10.1 ± 0.1	113.5	26.8	0.85	2.0
2500 (33)	TEOS	33.6	10.0 ± 0.2	87.9	26.5	1.24	2.4
6000 (80)	Vinyl	57.8	$10.34 \pm .05$	179	27.4	4.04	2.9
12000 (160)	Vinyl	127.6	10.06 ± 0.04	432	26.7	11.7	3.9
22000 (293)	Vinyl	153	9.9 ± 0.2	524.7	26.2	13.6	4.8
Falcao data							
4500 (60.5)	Radiation	78.1	11.7	261.2	31.0	5.25	2.8
15000 (200)	Radiation	143	10.6	489	28.1	13.3	4.3
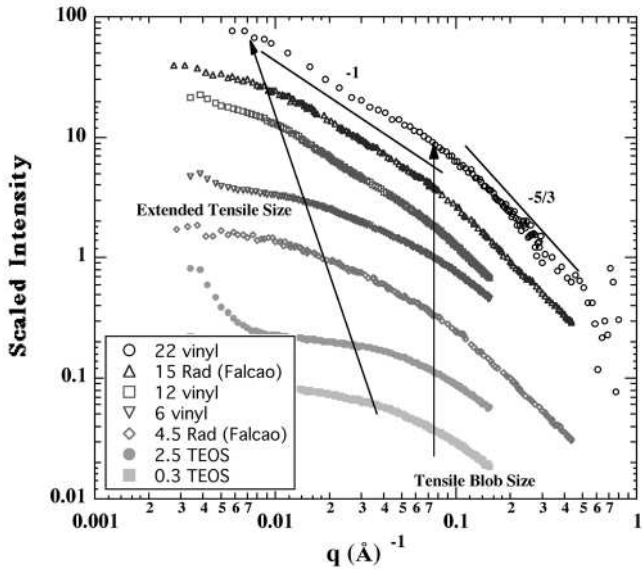
Fig. 3. Neutron scattering data from a series of equilibrium-swollen networks of PDMS of variable molecular weight between crosslinks. The legend shows the molecular weight between crosslinks in kg/mole. "vinyl" indicates hydrosilation crosslinking, "TEOS" indicates crosslinking by tetraethylorthosilicate and "Rad" indicates radiation crosslinking.

**Fig. 4.** Typical unified fit under the GTB model to an intermediate molecular-weight curve from Figure 3.

curves in Figure 2. Such plots are useful in showing the relative contributions to the unified scattering function. In this case the high-q structural level component is similar to the equivalent solution curve (the statistical error in R_g is given in the caption accompanying the figure). The errors reported for the fitting parameters are propagated from the statistical error in the intensity.

The scattering from a series of equilibrium-swollen PDMS networks were investigated as a function of the molecular weight between crosslinks, Figure 3. Through a comparison of this series, under the GTB model, it can be qualitatively seen that the gel tensile-blob size, ξ, associated with the knee in the data at about 0.08 Å^{-1}, remains fairly constant (vertical arrow in Fig. 3) across the series.

This is consistent with the prediction of the GTB model that ξ is independent of the molecular weight between crosslinks, as can be seen from equation (1). Owing to the limited data available in the high-q range for some of the samples, we refrain from commenting on any variations in the value of the scaling exponent. The extended length of the tensile blob structure, L, increases monotonically with the molecular weight between crosslinks for all the molecular weights studied. Detailed comparison with the prediction of the GTB model for L will be discussed below.

The structural sizes from unified fits are shown in Table 1. ξ is close to 27 Å for all samples independent of N_c and type of crosslinker. All experiments reported here, as well as those of Falcao *et al.* [13] (mentioned below), were run at close to 25 °C. Falcao *et al.* used p-xylene rather than benzene which yields a slightly larger value for ξ, ~ 30 Å. Falcao's networks were produced by radiation crosslinking rather than the end-linking reactions used in this study. A different internal dimension, D, and possibly even a different value of α, is expected for Falcao's
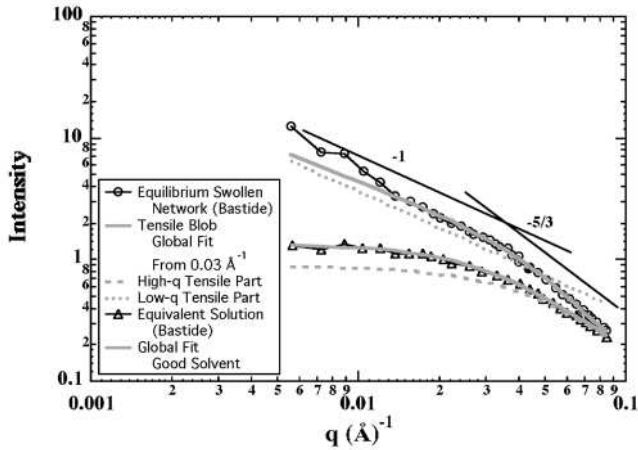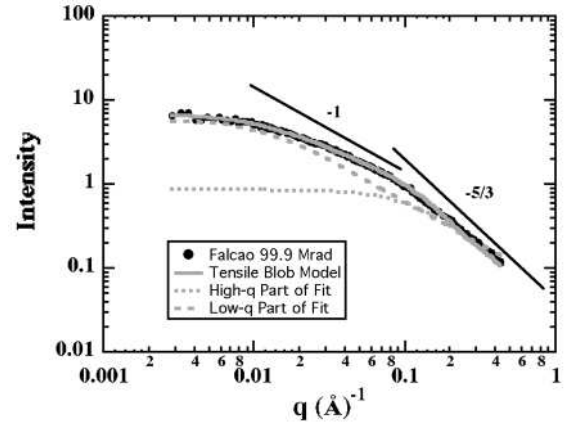
Fig. 5. GTB model fit to the data from Mendes *et al.* [18]. The sample is polystyrene of 22000 g/mole between crosslinks in deuterated toluene. The network is equilibrium swollen; the solution (lower curve) is an equivalent concentration of linear polymer.

network. Without a knowledge of the values of D and α, detailed comparison between the predictions of the GTB model (Eq. (1)) and the variation in the value of ξ obtained by using different solvents (d-benzene for our data and p-xylene for Falcao *et al.*'s data) is not possible. Studies using the same network swollen to equilibrium in several solvents, as well as temperature measurements, to determine the validity of equation (1) will be reported in the future.

Figure 5 shows a typical fit to one of the intermediate molecular-weight curves (6000 g/mole) for comparison with Figure 3. The dashed curves are the components of the unified fit associated with the tensile blobs (high q) and the elongated linear structure of Figure 1 (low q).

4.1 Comparison with literature data

Several other groups have previously reported neutron scattering data from equilibrium-swollen gels. We have examined the data of Mendes *et al.* [18], Figure 5, and Falcao *et al.* [16], Figures 6 and 7. In most cases good fits result using the 3-parameter unified function modified for the GTB model. Figure 5, for instance, shows a fit to the data of Mendes *et al.* for a polystyrene gel crosslinked with di-vinyl benzene ($f = 6$, $N_c = 212$) and the equivalent solution in deuterated toluene with $M_c = 22000$ with a polymer volume fraction of 0.0416 ($Q = 24$). The fits shown in Figure 5 yield an equivalent solution radius of gyration of 47.2 Å and a tensile-blob radius of gyration of 35.1 Å. The disagreement between these values further indicates that ξ does not correspond to the concentration blob. The extended chain radius of gyration, related to L, is not observable in the Mendes *et al.* data. The two components to the unified tensile-blob fit are shown (dashed curves). Using equation (4) and the fit value for the tensile-blob radius of gyration, ξ is calculated to be 93 Å. The observed ratio of ξ for the PS network and the PDMS is roughly 3.4. The higher functionality of crosslink

Fig. 6. GTB model fit to the data from Figure 9 in Falcao *et al.* [16]. 99.9 Mrad PDMS in d-para-xylene. Fit values are included in Table 1 ($N_c = 60.5$).
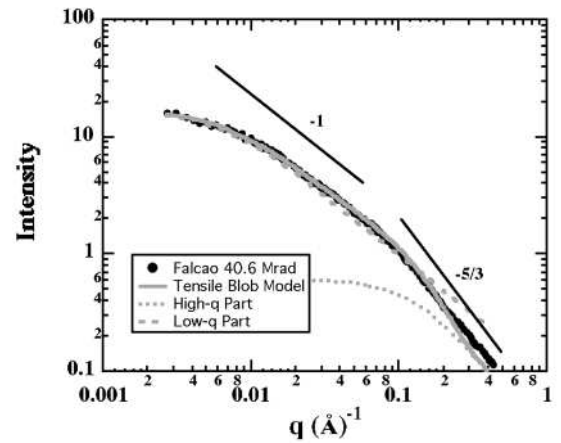

Fig. 7. GTB model fit to the data from Figure 9 in Falcao *et al.* [16]. 40.6 Mrad PDMS in d-para-xylene. Fit values are indicated in Table 1 ($N_c = 200$).

sites, $f = 6$ for the PS network *versus* $f = 4$ for end-linked PDMS again brings into question whether these two systems have equal values of the internal dimension, D, and α. Therefore, equation (1) cannot be verified by comparison of the Mendes *et al.* data and the data presented here due to expected differences in D and α. The large value of Q reported by Mendes *et al.*, coupled with the large observed value of ξ and the higher molecular weight between crosslinks for the network studied, makes the large L (larger than observable in the q range available in the Mendes *et al.* data) reasonable in the context of equation (2).

4.2 Calculations based on fits using the GTB model

Equation (2) indicates that the extended tensile length, L, scales with $L \sim Q^{1/2} N_{\mathrm{avg}}$ for a polymer network swollen in a solvent (fixed value of χ) and for fixed values of D and α. Figure 8 shows that this predicted power law behavior is supported by the data obtained on PDMS gels with the
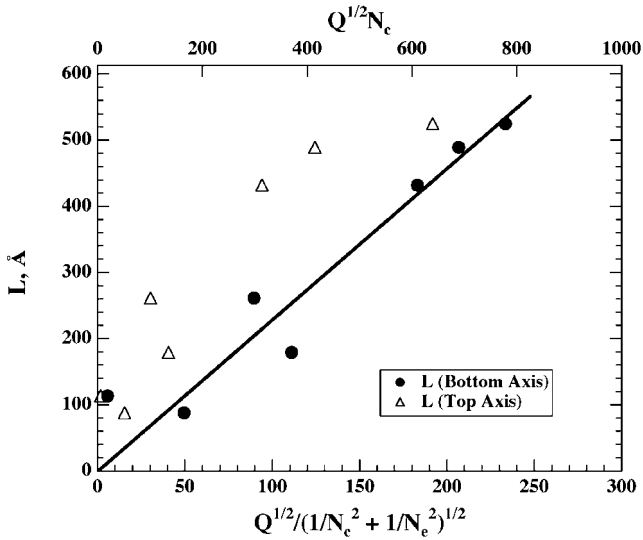
Fig. 8. Linear plot of extended tensile length *versus* the function suggested by equation (2). The bold line indicates the expected intercept at the origin. Empty triangles indicate the behavior when account is not made for topologically trapped entanglements (top axis).

Fig. 9. *L versus* $N_{\mathrm{avg}}^{(13/10)}$. The straight line passes through the origin as predicted by equation (12).

exception of the $N_{\mathrm{c}} = 4$ gel. This may be due to incomplete crosslinking in the $N_{\mathrm{c}} = 4$ gel. Equation (2) predicts that the curve in Figure 8 should pass through the origin and it can be seen that this is indeed the case. Correction for the entanglements brings the data points closer to a straight line at higher values of N_{c}, the last three data points to the right in Figure 8.

Flory-Rehner theory [1,3] predicts that $Q \sim N_{\mathrm{c}}^{3/5}$ while the c* theorem of de Gennes [2,3] suggests that $Q \sim N_{\mathrm{c}}^{4/5}$. It is now evident that N_{c} must be modified for entanglements and equation (2) suggests the function $N_{\mathrm{avg}} = \left(\frac{1}{f N_{\mathrm{c}}^2} + \frac{1}{4 N_{\mathrm{e}}^2} \right)^{-1/2}$. Then the expression,
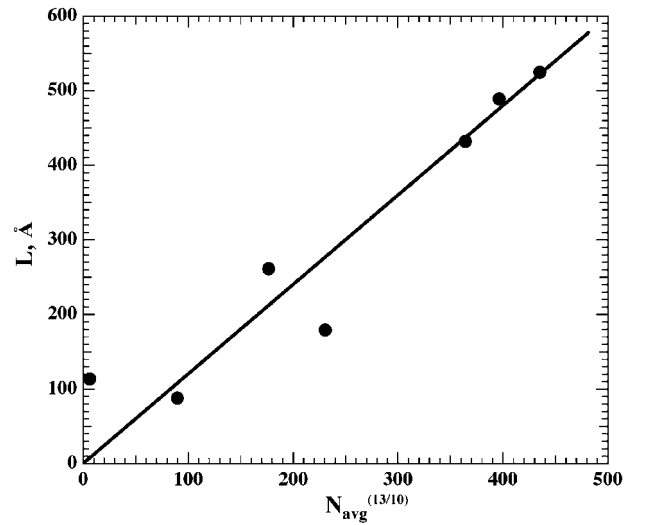
$$Q \sim N_{\mathrm{avg}}^{3/5} \tag{11}$$

can be used to obtain an approximate scaling relationship between L and N_{avg},

$$L \sim N_{\mathrm{avg}}^{13/10} . \tag{12}$$

Figure 9 shows a plot of L against $N_{\mathrm{avg}}^{13/10}$. As predicted by equation (12), we obtain a linear plot of slope 1 and the extrapolated line passes through the origin. Again, the lowest-molecular-weight sample diverges from the predicted behavior possibly due to incomplete crosslinking in this $N_{\mathrm{c}} = 4$ sample.

5 Conclusions

The GTB model coupled with the unified function gives a good description of small-angle neutron scattering patterns from equilibrium-swollen gels in many cases. The

scattering patterns exhibit two characteristic lengths associated with equilibrium-swollen gels, the gel tensile-blob size, ξ, and the extended tensile length, L, in agreement with the predictions of the model and contrary to classical theories of swelling behavior which predict just one characteristic size. In the high-q regime, *i.e.* above ξ, power law scattering was observed, consistent with the prediction that the gel tensile blob is a fractal object. The GTB model predicts constant ξ for constant connectivity (determined by D), constant interpenetration (determined by α), temperature, and solvent/polymer system and is independent of the molecular weight between crosslinks. In agreement with the model, ξ was found to be approximately constant for the series of molecular weights studied. The GTB model predicted that ξ is strongly sensitive to the two exponents, D and α. Due to a lack of sufficient q range in this region for some of the scattering curves we were unable to investigate the variation in the mass fractal dimension of the gel tensile blob. Even if sufficient q range were available so that we could unambiguously determine the mass fractal dimension of the gel tensile blob, that only yields the sum $D + \alpha$ and not the individual values of the exponents. Therefore, studying the dependence of ξ on the exponents D and α still presents a problem. One could imagine that the functional dependence of ξ on D could be investigated by comparing networks of the same polymer prepared at the same concentration in solution, with crosslinks of varying functionality. This should alter the connectivity of the network thereby changing D. The above scheme provides a way to isolate the effects of D on the mass fractal dimension. Further, a recent method [30] that allows a direct determination of the dimension of the minimum path of a fractal object from small-angle scattering data could prove useful in this regard. On the other hand, α can be systematically varied by preparing networks of identical functionality at different concentrations in solution. These studies have been planned for the future. The GTB model further predicts that ξ depends on

the Flory-Huggins interaction parameter, χ as given in equation (1). By varying the solvent used to swell the polymer network, we should be able to vary χ. Further, Flory predicted that $\chi \sim 1/T$ [1], implying that ξ is a function of the temperature, T. These dependencies remain to be verified and will be focus of future work.

Between ξ and L, the scattering pattern obeys the scattering law, $I(q) \sim q^{-1}$, in agreement with the predictions of the model. The GTB model provides an explanation for values of L larger than the mesh size of the network. Predictions of the model regarding the dependence of L on N_c and Q (as seen in Eq. (18)) were verified. Through the use of an average molecular weight between crosslinks, $N_{\text{avg}} = \left(\frac{1}{fN_c^2} + \frac{1}{4N_e^2} \right)^{-1/2}$, agreement is found with the basic predictions of Flory-Rehner theory. The effect of entanglements that are topologically trapped in the network can be seen by the dependence of L on N_e and this inclusion of the effect of entanglements can explain the saturation of the swelling ratio for high values of N_c.

One limitation of the GTB model in the current form is that it fails to provide a calculation of the swelling ratio in terms of the gel parameters. The proposed scaling dependence of the swelling ratio on the average molecular weight is heuristic. The problem will be investigated in the future. Future studies are also planned to explore the kinetics of gel swelling and deformed gels using the GTB model.

References

1. P.J. Flory, *Principles of Polymer Chemistry* (Cornell University Press, Ithaca, New York, 1953).
2. P-G. de Gennes, *Scaling Concepts in Polymer Physics* (Cornell University Press, Ithaca, New York, 1979).
3. J.P. Cohen Addad (Editor), *Physical Properties of Polymeric Gels* (Wiley, New York, 1996).
4. T. Tanaka, L.O. Hocker, G.B. Benedek, J. Chem. Phys. **59**, 5151 (1973).
5. F. Horkay, A.M. Hecht, E. Geissler, J. Chem. Phys. **91**, 2706 (1989).
6. F. Bueche, J. Colloid Interface Sci. **33**, 61 (1970).
7. E. Pines, W. Prins, J. Polym. Sci. B **10**, 719 (1972).
8. K.L. Wun, W. Prins, J. Polym. Sci. Polym. Phys. Ed. **12**, 533 (1974).
9. R.S. Stein, J. Polym. Sci. B **7**, 657 (1969); V.K. Soni, R.S. Stein, Macromolecules **23**, 5257 (1990).
10. J.G.H. Joosten, J.L. McCarthy, P.N. Pusey, Macromolecules **24**, 6690 (1991).
11. H. Benoit, D. Decker, R. Duplessix, C. Picot, P. Rempp, J.P. Cotton, B. Farnoux, G. Jannik, R. Ober, J. Polym. Sci. Polym. Phys. Ed. **14**, 2119 (1976).
12. M. Beltzung, J. Hertz, C. Picot, Macromolecules **16**, 580 (1983).
13. J. Bastide, R. Duplessix, C. Picot, S. Candau, Macromolecules **17**, 83 (1984).
14. E. Mendes, P. Lindner, M. Buzier, F. Boue, J. Bastide, Phys. Rev. Lett. **66**, 1595 (1991).
15. F. Horkay, A.M. Hecht, S. Mallam, E. Geissler, A.R. Rennie, Macromolecules **24**, 2896 (1991).
16. A.N. Falcao, J.S. Pedersen, K. Mortensen, Macromolecules **26**, 5350 (1993).
17. E. Geissler, F. Horkay, A.-M. Hecht, Phys. Rev. Lett. **71**, 645 (1993).
18. E. Mendes, A. Hakiki, A, Ramzi, J. Herz, F. Schosseler, J.P. Munch, F. Boue, J. Bastide, ACS Abstr. PMSE **205**, 127 (1993).
19. S.K. Sukumaran, G. Beaucage, Europhys. Lett. **59**, 714 (2002).
20. J. Bastide, L. Leibler, Macromolecules **21**, 2647 (1988).
21. A. Onuki, J. Phys. II **2**, 45 (1992).
22. S. Panyukov, Y. Rabin, Phys. Rep. **269**, 1 (1996).
23. T. Norisuye, N. Masui, Y. Kida, D. Ikuta, E. Kokufuta, S. Ito, S. Panyukov, M. Shibayama, Polymer **43**, 5289 (2002).
24. P. Pincus, Macromolecules **9**, 386 (1976).
25. G. Beaucage, S. Rane, S. Sukumaran, M.M. Satkowski, L.A. Schechtman, Y. Doi, Macromolecules **30**, 4158 (1997).
26. G. Beaucage, J. Appl. Crystallogr. **29**, 134 (1996).
27. G. Beaucage, J. Appl. Crystallogr. **28**, 717 (1995).
28. B. Viers, PhD Thesis, University of Cincinnati (1999).
29. A. Guinier, G. Fournet, *Small-Angle Scattering of X-rays* (Wiley, New York, 1955).
30. G. Beaucage, Phys. Rev. E **70**, 031401 (2004).